Determination of unbound states in ^{35}S from neutron total and capture cross-section measurements on ^{34}S

R. F. Carlton
Middle Tennessee State University, Murfreesboro, Tennessee 37132

W. M. Good, J. A. Harvey, R. L. Macklin, and B. Castel*
Oak Ridge National Laboratory, Oak Ridge, Tennessee 37831
(Received 23 January 1984)

The high neutron resolution capability of the Oak Ridge Electron Linear Accelerator has been used to investigate the unbound region of ^{35}S via neutron resonance spectroscopy studies of the ^{34}S+n system. The total cross section of ^{34}S was measured over the neutron energy range from 90 to 1500 keV, and the capture cross section was measured over the range from 30 to 1100 keV. Analysis of the data yielded spectroscopic factors for the s states in the unbound region for excitation energies from 7 to 8 MeV. Continuum shell model calculations of the s and d states were also performed for both the bound and the unbound regions of ^{35}S. In general, the measured and calculated neutron strengths for s waves in the unbound region are in reasonable agreement, although the fragmentation of single-particle strength seen experimentally is somewhat higher than that predicted. Core-particle calculations for the p states in the unbound region of ^{35}S were also performed, and, on the basis of all these results, plus those of others, we have summarized our understanding of the distributions of single-particle neutron strengths in the s, p, and d states of ^{35}S for excitation energies up to 8.5 MeV.

I. INTRODUCTION

Studies of the bound region of ^{35}S by means of the (d,p) reaction[1] have identified a total of 45 bound states (13 with firm J^π assignments), and the calculated distributions[2] of low-lying single-particle strengths have been shown to be in good agreement with the measured data. While the bound states of ^{35}S have thus been established, no similar detailed information has been available on the unbound levels in this nuclide. Studies have been made, however, of the unbound regions of nuclides that are near neighbors of ^{35}S. We have identified unbound states in ^{31}Si by using high-resolution neutron spectroscopy in the selective excitation and separation of contributions to unbound levels from s- and p-wave neutrons,[3] and other experimenters[4−7] have performed extensive studies of both the bound and unbound regions of ^{33}S by numerous reactions, one study[6] being very similar to the present investigation.

In addition, continuum shell model calculations have been performed[8] for the ^{33}S nuclide, and when the calculated results were compared with those from early elastic-scattering measurements on the ^{32}S+n system,[9] sufficient agreement for s-wave resonances was obtained to assign the theoretical doorway state configurations to specific groups of resonances in the system. However, the prediction[8] that direct-semidirect capture by ^{32}S would be important was not supported by later measurements.[6] In fact, little valency capture was observed for $p_{1/2}$ resonances. In contrast, the prediction[10] of direct capture for ^{34}S does appear to be confirmed by measurements of partial capture cross sections for thermal neutrons in the

^{34}S(n,γ)^{35}S reaction,[11] indicating that differences exist in the nuclear structures of ^{32}S and ^{34}S. This is supported by the fact that the quadrupole moments of the two nuclides are known to differ (-11.5 ± 4.8 for ^{32}S; 6.3 ± 4.3 for ^{34}S).[12]

These differences in the ^{32}S and ^{34}S nuclides provided the incentive for the combined experimental and theoretical study of the unbound region of ^{35}S described here. Measurements of neutron transmission and capture measurements for ^{34}S were performed at the Oak Ridge Electron Linear Accelerator (ORELA) by the same technique employed in earlier studies,[3,6] and the data were analyzed to obtain neutron strengths of resonances in the 7- to 8.5-MeV excitation region of the unbound region of ^{35}S. In addition, continuum shell model calculations were performed to determine s and d states for both the bound and the unbound regions of ^{35}S and core-particle calculations were performed to obtain p states for the unbound region. On the basis of all these results, plus those of others, we summarize our understanding of the distributions of single-particle neutron strengths in s, p, and d states in ^{35}S for excitation energies up to 8.5 MeV.

II. CROSS-SECTION MEASUREMENTS

A. Total cross section

The total cross section of ^{34}S was measured at ORELA over the neutron energy range from 90 keV to 1.5 MeV, the overall experimental technique having been described in detail in an earlier paper.[13] During these measurements the ORELA operating conditions were maintained at an

800-Hz pulse repetition rate, a 5-ns burst width, and a 10-kW average beam power. The energy resolution $\Delta E/E$ was $\simeq 10^{-3}(1+3E)^{1/2}$, where E is in MeV. The ^{34}S sample was positioned 9 m from the water-moderated tantalum target, and the neutron detector (a 2-cm-thick, 7.5-cm-diam NE-110 proton-recoil detector) was located at a flight path of 78 m. At the sample position, the neutron beam was collimated to a diameter of 1.6 cm.

The sample was 94.33%-enriched ^{34}S with a 5.54% impurity of ^{32}S. It weighed 14.96 g and had a thickness of 0.0811 atoms of ^{34}S per barn. Data were obtained with the sample container and an identical empty container alternately cycled in and out of the neutron beam. For a given sequence, the sample-in/sample-out ratio was normalized to a neutron monitor to compensate for variation of the neutron production rate. The total cross section of ^{34}S after correction for the dead time of the time digitizer and backgrounds is shown in Fig. 1.

B. Capture cross section

The neutron capture cross section of ^{34}S was measured over the neutron energy range from 30 to 1100 keV by the
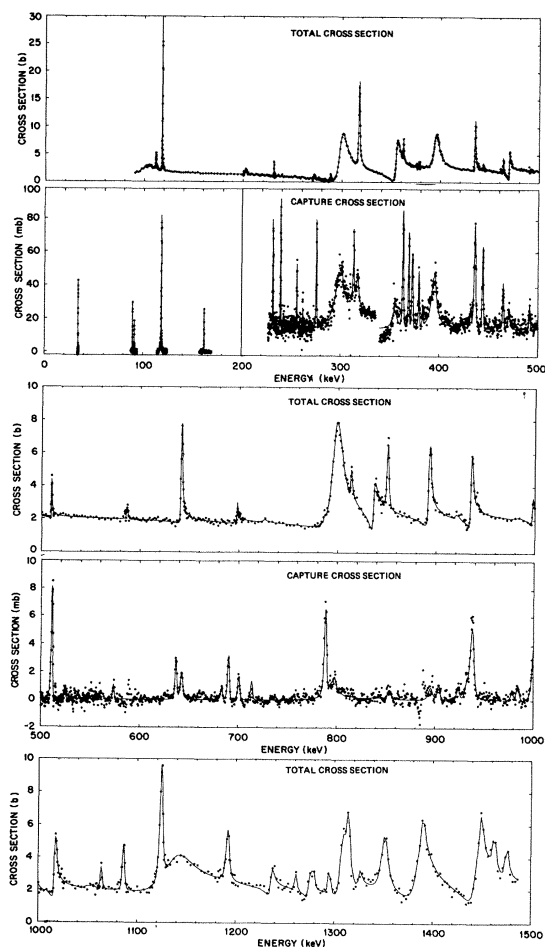
FIG. 1. Total cross section of ^{34}S from 90 to 1500 keV and capture cross section from 30 to 1000 keV. Above 200 keV, the capture data are plotted from -2 to 10 mb. The solid lines are the results of fitting by the parameters listed in Tables I and III.

same technique as that described for the ^{33}S study.[6] For these measurements, the ORELA operating conditions were maintained at an 800-Hz pulse repetition rate, a 4-ns burst width, and a 13-kW average beam power for 120 h. Time-dependent neutron backgrounds, determined by "black resonance" filters, were less than 1%. The neutron flux was monitored by a thin (0.5 mm) ^{6}Li glass scintillator, which had been calibrated[14] against a ^{235}U fission chamber. The flux monitor was placed in the neutron beam approximately 40 cm ahead of the sample, which was located at a flight path distance of 40 m.

The sample, made from the material used for the total cross-section measurements, weighed 14.95 g and had a thickness of 0.1834 atoms of ^{34}S per barn. Two nonhydrogenous fluorocarbon scintillators (NE-226) with a combined solid angle of approximately 2π were used to measure the neutron capture rate by means of the total energy weighting technique.[15] The measured total energy loss was corrected for a calculated 3.4% energy loss in the sample. Normalization of the calculated detection system efficiency to that of the neutron flux monitor was accomplished by saturation of the 4.9-eV resonance in ^{197}Au$+$n.

The capture data were corrected for various backgrounds, including sample-dependent and sample-independent beam-induced backgrounds. Compensation for the latter was accomplished by subtraction of a normalized no-sample run made under similar operating conditions. Sample-dependent background corrections were modeled by a combined $E^{-1/2}$ component and a resonance structure component from known capture resonances which arise in the detection apparatus (induced by neutrons scattered from the sample). Corrections were then made for ^{32}S impurity contributions to the measured capture cross section by a linear subtraction based on a previous measurement[6] of the ^{32}S capture cross section over the same energy range. The resulting capture cross section of ^{34}S is included in Fig. 1.

III. DATA ANALYSIS METHODS

A. Total cross section

The Doppler- and resolution-broadened transmission data were analyzed with the code SAMMY,[16] which uses the multilevel R-matrix formalism with the Reich-Moore approximations. For the single-channel case, the R matrix reduces to an R function, namely

$$R(E) = R^{\text{ext}}(E) + \sum_{\lambda=1}^{N} \gamma_\lambda^2/(E_\lambda - E - i\Gamma_\lambda/2) , \qquad (1)$$

where the R^{ext} component is due to the levels outside the analyzed region. R^{ext} is important not only for fitting the data between resonances but also for fitting the resonance asymmetries arising from interference between resonance scattering and potential scattering plus R^{ext} for each partial wave. Therefore, R^{ext} can be obtained for all l,J values for which observable asymmetries exist.

For R^{ext}, one may choose either a pole representation or a parametrization described by Johnson and Winters.[17] We chose the latter, which expresses R^{ext} as

$$R_{Jl}^{\text{ext}}(E) = \widetilde{R}_{Jl}(E) - \langle \gamma_\lambda^2 / D \rangle_{Jl} \ln \left| \frac{E_u - E}{E - E_l} \right| , \qquad (2)$$

where E_l and E_u are the limits of the analyzed region and $\langle \gamma_\lambda^2 / D \rangle$ is the neutron strength function. (A detailed elaboration of this formulation has been recently published.[18])

The Johnson-Winters formulation provides a good approximation to the average scattering function, which is related to the phenomenological optical model. The log term in the expression corresponds to a uniform distribution of strength outside the region of analysis. We have used a value for this uniform external strength equal to the average strength inside the region of analysis. The other term, R_{Jl}, is parametrized as $\alpha_{Jl} + \beta_{Jl}E$. With a constant $\langle \gamma^2 / D \rangle$, the parameters α and β may be varied in fitting nonresonant contributions. Initially, a value of $\langle \gamma^2 / D \rangle$ is estimated and approximate resonance parameters are obtained. A new value is then computed from these parameters and final resonance and external parameters are determined. Contributions from the ^{32}S contamination were parametrized in a similar manner (using values from the previous study[6]) and were held fixed throughout the analysis.

The analysis was carried out over the neutron energy range from 90 to 1500 keV and included approximately 2500 data points. Though computing constraints required that the data be broken into three separate sets for sequential analysis, the results obtained are equivalent to a simultaneous analysis since the input to each data set consisted of the output parameters and covariances from the prior data set. Thus, the results for the entire region are self-consistent.

The quantities not varied in the present analysis included the channel radius (4.37 fm) and the radiation widths. The latter were held fixed at the values obtained from the capture analysis (see below) in those cases where definitive J^π assignments were possible. Radiation widths of other resonances were assumed to have a value of 0.67 eV. The computed contributions for the ^{32}S contamination from the known parameters[6] of ^{32}S+n agreed with the experimental data, thus providing an internal consistency check on the sample composition.

B. Capture cross section

The capture data have been analyzed with the code LSFIT,[19] which carries out a least squares fitting to a Breit Wigner expression to extract the parameters E_0 and Γ_γ for resonances observed in transmission. The program applies corrections for Doppler and resolution broadening, resonance self-protection, and multiple scattering and can fit a region containing up to 15 resonances and 500 data points.

The resolution function includes a convolution of a low-energy asymmetric tail with a primary Gaussian component. For resonances superimposed on the side of a larger resonance, proper off-resonance scattering cross sections, given by the transmission data, were used, together with the capture cross section of the larger resonance (at the appropriate energy), for the background con-

tribution to the smaller resonance. The sensitivity of the detector to prompt neutrons scattered from the sample required a correction to the radiation widths deduced from the fitting. The correction is of the form $\Gamma_{(\text{cor})} = \Gamma_\gamma - c\Gamma_n$, where c is an energy-dependent correction factor that varies from 10^{-3} to 10^{-4} in the energy range of this analysis. This correction is significant only for the broadest resonances. The results of the capture measurements and analysis are included in the table of resonance parameters (see Table I). When resonances were observed in both the transmission data and the capture data, the energies of the resonances were taken from the transmission measurements.

IV. DATA ANALYSIS RESULTS

A. Resonance parameters

A total of 81 resonances were observed in this study. Of these, 48 were analyzed in transmission to obtain resonance energies (E_n) and neutron widths $(g\Gamma_n)$. They were also analyzed in capture, with favorable cases leading to a determination of both the neutron width and the radiation width (Γ_γ). For the 33 resonances seen in capture with neutron widths below the detection limit of the transmission measurement, we were able to deduce only the capture kernel $g\Gamma_n\Gamma_\gamma / \Gamma$. The resulting resonance parameters, presented in Table I, are based upon capture data below 116 keV, upon combined capture and transmission data up to 1.02 MeV, and upon transmission data alone at higher energies.

Whenever possible, the resonance energies given in Table I are based upon transmission analysis results. In the other cases they are based upon a normalization to that energy scale. The uncertainties on E_n, computed by the fitting code, are based upon uncertainties in the path length and flight time.

In most cases the uncertainties on the neutron widths represent statistical errors propagated by the code through the fitting process and do not include systematic errors, which are less than 2%. In other cases, the sensitivity of this parameter to trial and error adjustment was used to estimate the uncertainty. For those resonances seen only in capture, an upper limit on the neutron width was estimated with no associated uncertainty.

The radiation widths given in Table I are defined only for resonances seen in both the transmission measurements and the capture measurements. The quoted uncertainties are based upon the combination in quadrature of statistical uncertainties on Γ_γ and the 50% uncertainty on the neutron sensitivity correction factor. The values deduced from the capture analysis were held constant in a transmission reanalysis.

Finally, as noted in Table I, J^π assignments to the resonances were made on the basis of the following considerations:

(a) For those resonances whose widths are large compared to the overall resolution, the J assignments were made through comparison of the observed peak-to-valley cross section with the expected peak-to-valley cross section for the assumed J. Furthermore, the parity for these

resonances was established and the J assignment was corroborated by the extent of the interference minimum for a given J^π. These asymmetries may be due to both resonance potential scattering interference and, depending on the choice of channel radius, to interference between the resonance and the R^{ext} of the assumed J. For those resonances in which pronounced asymmetries occur, one thus gains additional information regarding the contributions

from the external region.

(b) For smaller resonances showing asymmetry, the J assignments were based on the asymmetries.

(c) For small isolated resonances lacking obvious asymmetry, we used the single-level program DCON (Ref. 20) in fitting for various assumed J values and compared the computed phase shifts with those expected from energy trends in the phase shifts for given partial waves.

TABLE I. Resonance parameters for the ^{34}S+n reaction. The J assignments are based on the following: (A) Peak-to-valley cross section; asymmetry. (B) Asymmetry. (C) Phase shift trends. (D) Reduced width considerations. (E) Porter-Thomas considerations.

E_n (keV)	$g\Gamma_n$ (eV)	$g\Gamma_n\Gamma_\gamma/\Gamma$ or Γ_γ (eV)	J^π	E_n (keV)	$g\Gamma_n$ (eV)	$g\Gamma_n\Gamma_\gamma/\Gamma$ or Γ_γ (eV)	J^π
34.03(1)[a]		0.025(1)[b]	$l=2$ (E)	698.2(1)	305(50)	0.80(8)	$l=1,2$ (D)
89.40(3)		0.14(4)[b]		713.0(7)	<4	0.45(7)[b]	
91.12(4)		0.084(3)[b]		767.3(7)	<4	0.31(13)[b]	
115.2(3)		0.009(3)[b]	$l=2$ (E)	786.5(4)	18(6)	2.65(18)	
117.4(2)	<1	0.033(5)[b]	$l=2$ (E)	798.65(6)	25350(300)	1.52(50)	$\frac{3}{2}^-$ (A)
118.30(1)	372(3)	0.70(4)	$\frac{3}{2}^-$ (A)	813.8(1)	860(60)	0.19(13)	$\frac{1}{2}^-$ (B)
162.1(1)	<1	0.42(1)[b]		836.27(8)	3600(160)	0.39(18)	$\frac{1}{2}^+$ (B)
231.25(2)	62(4)	0.30(2)	$l=1,2$ (D)	850.94(6)	2650(110)	0.24(19)	$\frac{3}{2}^+$ (A)
239.0(4)	<4	0.33(2)[b]		893.17(6)	4950(160)	0.38(16)	$\frac{3}{2}^-$ (A)
255.5(5)	<4	0.19(1)[b]		902.0(12)	<3	1.13(19)[b]	
261.5(6)	<2	0.06(2)[b]		921.5(12)	<20	0.67(17)[b]	
275.3(6)	<1	0.35(2)[b]		930.0(12)	<20	0.57(25)[b]	
298.70(3)	9600(150)	2.82(67)	$\frac{1}{2}^+$ (B)	935.78(6)	4100(160)	3.48(23)	$\frac{3}{2}^-$ (A)
(302)		0.10(3)[b]		941.0(3)	176(16)		
313.0(8)	<6	0.31(3)[b]		976.4(15)	<2	0.5(3)[b]	
317.51(5)	2500(25)	0.23(8)	$\frac{3}{2}^-$ (A)	982.0(15)	<8	0.89(4)[b]	
355.41(2)	4810(80)	0.30(30)	$\frac{1}{2}^+$ (B)	997.9(1)	930(80)	3.51(19)	$\frac{3}{2}^-$ (C)
362.8(2)	230(10)	1.06(7)	$l=1,2$ (D)	1017.7(1)	4020(180)	1.22(17)	$\frac{3}{2}^-$ (A)
368.7(2)	<2	0.72(3)[b]		1064.4(2)	1032(90)		$l=2$ (B)
372.1(5)	<2	0.44(6)[b]		1086.7(2)	2650(160)		$l=2$ (B)
372.8(5)	<2	0.30(5)[b]		1123.0(2)	5480(388)		$l=2$
379.0(5)	<10	0.44(4)[b]		1124.5(3)	4730(320)		$l=2$
382.8(5)	<6	0.16(4)[b]		1140.0(5)	34880(830)		$\frac{1}{2}^-$ (B)
396.14(4)	6430(150)	3.08(20)	$\frac{1}{2}^-$ (B)	1192.2(2)	5510(290)		$l=2$ (B)
(397.6)		0.12[b]		1237.0(3)	2945(230)		$\frac{1}{2}^-$ (B)
422.3(6)		0.44(33)[b]	$l=2$ (E)	1261.8(3)	975(86)		
431.2(6)	<1	0.21(5)[b]		1275.1(4)	2170(180)		$\frac{1}{2}^-$ (B)
435.4(1)	1570(40)	0.91(8)	$\frac{3}{2}^-$ (A)	1279.4(4)	1140(100)		$l=2$ (B)
438.35(5)	49(5)			1295.5(3)	1980(150)		$l=2$ (B)
443.45(1)	80(8)	0.51(5)		1308.2(2)	12475(770)		$\frac{3}{2}^-$ (A)
456.4(6)	<6	0.12(3)		1314.5(4)	6240(500)		$\frac{5}{2}^+$ (A)
461.01(2)	50(5)	0.035(20)		1325.7(4)	1635(145)		$(\frac{1}{2}^-)$ (B)
463.9(4)	296(30)	0.28(3)	$l=1,2$ (D)	1351.4(3)	14470(650)		$l=2$ (B)
469.85(2)	1050(35)	0.37(8)	$\frac{1}{2}^+$ (B)	1388.0(4)	28845(1057)		$\frac{3}{2}^-$ (A)
490.5(6)	50(10)	0.33(4)[b]		1390.1(4)	1955(170)		$l=2$ (B)
510.02(4)	375(25)	2.1(1)	$\frac{1}{2}^-$ (B)	1447.2(4)	27100(1390)		$\frac{3}{2}^-$ (A)
523.8(6)	<4	0.17(4)[b]		1449.6(3)	3025(260)		$l=2$ (B)
573.0(6)	<1	0.21(3)[b]		1462.9(3)	3885(345)		$l=2$ (B)
636.5(6)	<10	0.90(8)[b]		1475.5(4)	3795(340)		$l=2$ (B)
641.93(3)	2520(60)	0.51(6)	$\frac{3}{2}^-$ (A)				
682.7(6)	<30	0.21(3)[b]					
689.7(6)	<10	0.80(5)[b]					

[a]In this notation, $34.03(1)\equiv34.03\pm0.01$.
[b]The value for the capture kernel, $g\Gamma_n\Gamma_\gamma/\Gamma$.

TABLE II. Average resonance parameters for the ^{34}S+n reaction.

J	D_{Jl} (keV)	$\langle \Gamma_n^l \rangle$ (eV)	$\langle \Gamma_\gamma \rangle$ (eV)	S_{Jl} ($\times 10^{+4}$)	Correlation $(\Gamma_n, \Gamma_\gamma)$	No. of resonances
$\frac{1}{2}^+$	180 ± 50	8 ± 6	1.0 ± 0.6	0.4 ± 0.3	$0.91^{+0.09}_{-0.14}$	4
$\frac{1}{2}^-$	135 ± 30	15 ± 9	1.3 ± 0.4	1.1 ± 0.6	0.49 ± 0.06	7
$\frac{3}{2}^-$	112 ± 19	10 ± 5	1.2 ± 0.3	0.9 ± 0.4	-0.23 ± 0.04	12
$l=1$	67 ± 8	12 ± 5	1.2 ± 0.3	0.9 ± 0.3	0.15 ± 0.04	19
$l=2$	22 ± 2	5 ± 2	0.67 ± 0.05	1.1 ± 0.5	-0.15 ± 0.03	58

(d) For some resonances, lower limit J assignments were established by average reduced width and strength function arguments, the assumption being that an assumed J assignment for a given $g\Gamma_n$ should not result in a reduced neutron width Γ_n^l exceeding the average for other similar J resonances by more than a factor of ~ 10. The remaining levels are too narrow for any assignment.

(e) Four resonances seen only in capture have unusually small ($\simeq \frac{1}{20}$ the average) kernels. These kernels are essentially $g\Gamma_n$, since radiation widths are not expected to vary by factors of 20. By assuming Porter-Thomas distributions with the observed population averages for s- and p-wave reduced neutron width, we find that there is a less than $\simeq 1\%$ probability that the resonances would be s or p wave. We have thus assumed an $l=2$ assignment in these cases.

Spectroscopic factors C^2S for the s-wave resonances given in Table I were computed from the expression

$$C^2S = \theta_n^2/\theta_{sp}^2 , \qquad (3)$$

in which

$$\theta_n^2 = \frac{\Gamma_n}{2P_l} \cdot \frac{mR^2}{\hbar^2}$$

is evaluated for the assumed channel radius, and θ_{sp}, the $2s$ dimensionless single particle width, is taken to be 0.175 (derived in Ref. 21 for the case of s states in ^{13}C). These experimental spectroscopic factors are compared with calculated values in Sec. V below.

B. Average resonance properties

From the deduced neutron widths of a given J^π, we calculated the strength functions from the expression

$$S_{Jl} = \langle \Gamma_n^l \rangle_J/D_{Jl} , \qquad (4)$$

where D_{Jl} is the average level spacing for a given spin and parity, and the reduced neutron width Γ_n^l is calculated from the expression

$$\Gamma_n^l = kR\Gamma_n/P_l\sqrt{E_0} , \qquad (5)$$

where $R = 1.35A^{1/3}$ fm and E_0 is in eV. In calculating the average, we made a correction ($\sim 10\%$) for the estimated number of resonances missed for each J^π, the correction being based on an assumed Porter-Thomas distribution of the reduced neutron widths and an estimate of the experimental sensitivity for determining small resonances.

The resulting averages for s-, p-, and d-wave resonances are summarized in Table II. The strength functions agree with those obtained for ^{32}S+n and are in good agreement with optical model predictions in this mass region. The average total radiation widths of the four $s_{1/2}$, seven $p_{1/2}$, and twelve $p_{3/2}$ resonances are 1.0 ± 0.6, 1.3 ± 0.4, and 1.2 ± 0.3 eV, respectively. The dispersion of the observed radiation widths about their respective means, assuming a chi-squared distribution, implies one degree of freedom for s-wave radiation widths and three degrees of freedom for p-wave capture. In addition, a high value of 0.91 for the correlation coefficient ρ is obtained between neutron and radiation widths for s-wave resonances, which suggests a direct component to the capture. However, there is a 8.5% probability of equaling or exceeding this value for ρ if the widths are uncorrelated. In the case of p-wave capture, the three degrees of freedom suggests that the decay from these capturing states is dominated by a few ($\simeq 3$) primary gamma rays.

C. External R function

In favorable cases, the important external R function can be deduced for the various partial waves from the neutron total cross-section measurements. Since the contribution of distant levels of a given J^π is closely connected to the average scattering function, one may thus investigate the l dependence of the real part of the low-energy optical potential.[17,18,22] In the case of ^{32}S, an l dependence of the real well depth was found. The implications for ^{34}S and ^{30}Si will be the subject of a later paper on systematic trends in this regard for neighboring nuclei.

For s waves, the external R function has historically been related to the elastic scattering length R' through the expression

$$R' = a[1 - \tilde{R}(E=0)] , \qquad (6)$$

where a is the channel radius. We obtained a value of 3.46 fm for R', which is in good agreement with the value of 3.6 fm deduced[23] from low-energy scattering measurements.

The fitted values for the external R function parameters are presented in Table III [see also the discussion following Eq. (2)]. The listed uncertainties for α_{Jl} are based upon the independent variation of this parameter required to produce a clearly unacceptable fit to the region for which that parameter is most important. Uncertainties for β_{Jl} are not listed since these parameters are highly correlated with the $\langle \gamma^2/D \rangle$, whose uncertainties are taken from the resonance analysis.

TABLE III. External R function parameters for the ^{34}S+n reaction ($a = 4.37$ fm).

l_J	α_{Jl}	β_{Jl} (MeV^{-1})	$\langle \gamma^2/D \rangle$
$s_{1/2}$	0.21 ± 0.03	0.01	$0.024^{+0.020}_{-0.011}$
$p_{1/2}$	-0.66 ± 0.10	0.25	$0.053^{+0.028}_{-0.018}$
$p_{3/2}$	-0.24 ± 0.05	-0.09	$0.050^{+0.019}_{-0.014}$

V. CALCULATIONS AND DISCUSSION
A. Positive parity states

As noted above, the bound region of ^{35}S has been studied extensively via the (d,p) reaction,[1] and the measured states have been shown to be in good agreement with calculations.[2] Spin and parity assignments have been made for 13 states with excitation energies up to 5.060 MeV, the most definitive from ^{34}S(d,p) measurements with polarized deuterons.[24] It was concluded that the $d_{3/2}$ strength was exhausted by the ground state, and, indeed, no other $\frac{3}{2}^+$ states were found. Furthermore, little $d_{5/2}$ strength was observed in the (d,p) measurements, and the strength that was found was shared between two states at 2.71 and 3.42 MeV (see Table IV).

The calculations for the bound states were shell model calculations. In this study, we also performed shell model calculations for the bound region of ^{35}S, and Table IV shows that our calculated results are in reasonable agreement with the s and d strengths observed in the measurements. In addition, we extended the shell model calcula-

tions to the unbound region covered by the ^{34}S+n reaction by using the modified surface delta interaction (MSDI) in the full $2s$-$1d$ space. At 680 keV, one $l=0$ is predicted to have a spectroscopic strength of $C^2S = 0.029$. This state has two-thirds of the combined strength of the four s-wave resonances observed in the $E_n = 90$—1500-keV region, which is also in satisfactory agreement. However, the shell model does not provide sufficient fragmentation for the $l=0$ strength.

B. Negative parity states

Analysis of the ^{34}S(d,p) measurements showed that three transitions leading to $J = \frac{7}{2}^-$ states exhausted the sum rule for $1f_{7/2}$ transitions.[24] This was not the case for the $p_{1/2}$ and $p_{3/2}$ states, however, which indicated the possibility of higher excited $2p_{1/2}$ and $2p_{3/2}$ states. This conclusion was confirmed by the observation of p-wave resonances in the present study in the $E_n = 90$—1500-keV region.

Since the shell model calculations were restricted to the $2s$-$1d$ space, they could not predict negative parity states in the unbound region of ^{35}S. The negative parity spectrum was therefore calculated in the core-particle framework similar to that used in the ^{32}S+n calculations.[8] Briefly, the nuclear wave function is expanded in terms of a complete set of eigenfunctions of an unperturbed Hamiltonian H_0,

$$\psi_E = \sum_{i=0}^{M} b_i(E)\phi_i + \int dE \, a_c(E)\chi_E \,, \tag{7}$$

TABLE IV. Experimental and calculated (shell model) positive parity states in ^{35}S.

Level	$E_x{}^a$ (keV)	E_{SM} (keV)	J^π	C^2S^b Expt (d,p)	C^2S^b Calc (SM)
Bound	0	0	$\frac{3}{2}^+$	0.48	0.30
	1572	1650	$\frac{1}{2}^+$	0.18	0.12
	2718	2110	$\frac{5}{2}^+$	0.02	0.02
	3421	2960	$\frac{5}{2}^+$	0.03	0.01

Level	$E_x{}^a$ (keV)	E_{SM} (keV)	J^π	C^2S^c Expt (n,n)	C^2S^c Calc (SM)
Unbound	7276.17(11)^d		$\frac{1}{2}^+$	0.024	
	7331.26(10)		$\frac{1}{2}^+$	0.012	
	7442.43(10)		$\frac{1}{2}^+$	0.002	
		7666			0.029
	7798.38(13)		$\frac{1}{2}^+$	0.005	
	7812.63(12)		$\frac{3}{2}^+$		
	8262.94(41)		$\frac{5}{2}^+$		

^aE_x is the excitation energy. The bound state values are from Ref. 1. Values for the unbound states were obtained using recoil-corrected neutron resonance energies and the value of 6986.00(10) keV for the neutron separation energy, obtained from Ref. 25.

^{b}Spectroscopic factor. Experimental (d,p) values were taken from Ref. 24.

^{c}See the text for the assumptions inherent in the expression used in calculating the spectroscopic factors from the measured neutron widths.

^{d}In this notation, 7276.17(11)$\equiv$7276.17$\pm$0.11.

TABLE V. Experimental and calculated (core particle) strength of unbound p states in ^{35}S.

Unbound states	$E_x{}^a$ (keV)	E_{CP} (keV)	J^π	Γ_n^l (eV) Expt	Calc
$p_{1/2}$	7370.82(11)^b		$\frac{1}{2}^-$	41.0	
		7431			26.5
	7481.44(11)			1.7	
	7776.55(14)			2.3	
	8093.43(51)			65.7	
	8187.66(32)			5.1	
	8224.67(41)			3.7	
		8256			39.4
	8273.82(41)			2.7	
		8566			28.2
				122.2	94.1
$p_{3/2}$	7100.92(10)		$\frac{3}{2}^-$	11.6	
	7294.44(11)			10.2	
	7408.96(14)			4.4	
		7451			18.9
	7609.59(10)			4.5	
	7761.83(11)			35.5	
	7853.65(12)			6.2	
	7895.04(12)			4.7	
	7955.39(14)			1.0	
	7974.62(14)			4.6	
		8066			41.2
		8246			36.9
	8256.82(22)			9.9	
	8334.34(41)			22.0	
	8391.85(41)			20.1	
				134.7	97.0

$^a E_x$ is the excitation energy, obtained using recoil-corrected neutron resonance energies and the value of 6986.00(10) keV for the neutron separation energy obtained from Ref. 25.
^{b}In this notation, 7370.82(11)$\equiv$7370.82$\pm$0.11.

where the ϕ_i's are bound states and the χ_E's are unbound states with one nucleon in the continuum. The choice of configurations for ϕ_i and χ_E is restricted to one-particle continuum states coupled to ^{34}S phonon states. The Schrödinger equation for the nuclear wave function is then solved by including only continuum-bound state coupling to first order. The photon field H' is also treated in a first-order approximation, and the S matrix for neutron capture to a final state ϕ_F becomes

$$S = \sqrt{2\pi\rho/\hbar}\langle \phi_F \mid H' \mid \psi_E \rangle \, , \tag{8}$$

where ρ is the density of states.

The resulting calculated spectroscopic factors for the $p_{1/2}$ and $p_{3/2}$ low-lying states in ^{35}S were in good agreement with the experiment, and the calculated $p_{1/2}$ strength is in reasonable agreement with the observed strength (see Table V). Three $p_{3/2}$ states are predicted in the $E_n = 0-1600$-keV region, and indeed several strong states are observed, as well as other states with smaller strengths.

strengths of many states in the unbound region of ^{35}S for excitation energies from 7 to 8.5 MeV. Our comparison with theory shows that both the shell model and the core-particle model yield particle strengths in the correct energy region and the calculated strengths are in reasonable agreement with those observed experimentally. Both models, however, use a restricted particle space and the effect of this restriction is seen in the lack of fragmentation obtained. The total $l=0$ and 1 strengths seen in ^{32}S+n and ^{34}S+n are roughly equal. The strength for s waves is an order of magnitude below the value of nuclides in the region of the $3s_{1/2}$ size peak, but in good agreement with optical model prediction of trends in this region.[21] The values from the sulfur studies help define the valleys approaching the $3s$ and following the $2p$ size resonances for which little experimental information is available. Finally, we should note the high degree of correlation between neutron and radiation widths, which suggests the possible presence of valence contributions to s-wave interactions in this nucleus.

VI. CONCLUSIONS

We have used the high resolution capability of the neutron resonance reaction to measure the total and capture cross sections of ^{34}S and to determine the locations and

*Permanent address: Department of Physics, Queen's University, Kingston, Ontario, Canada K7L 3N6.

[1]P. M. Endt and C. Van der Leun, Nucl. Phys. A310, 1 (1978).

[2]B. H. Wildenthal, J. B. McGrory, E. C. Halbert, and H. D. Graber, Phys. Rev. C 4, 1708 (1971).

[3]J. A. Harvey, W. M. Good, R. F. Carlton, B. Castel, and S. Mughabghab, Phys. Rev. C 28, 24 (1983).

[4]R. E. Peterson, H. H. Barschall, and C. K. Bockelman, Phys. Rev. 79, 593 (1950).

[5]S. Cierjacks, P. Forti, D. Kopsh, L. Kroop, J. Nebe, and H. Unseld, Kernforschungszentrum, Karlsruhe, Report No. EANDC (E)-III "U," 1968 (unpublished).

[6]J. Halperin, C. H. Johnson, R. R. Winters, and R. L. Macklin, Phys. Rev. C 21, 545 (1980).

[7]C. R. Jungmann, H. Weigmann, L. Mewissen, F. Poortmans, E. Cornelis, and J. P. Theobald, Nucl. Phys. A386, 287 (1982).

[8]D. Halderson, B. Castel, and G. Aizer, J. Phys. G 6, 59 (1980).

[9]M. Divadeenam (private communication), data shown in Ref. 8.

[10]A. M. Lane and J. E. Lynn, Nucl. Phys. 17, 563 (1960); 17, 586 (1960).

[11]R. F. Carlton, S. Raman, and E. T. Jurney, in Neutron Capture Gamma-Ray Spectroscopy, edited by T. von Egidy, F. Gonnenwein, and B. Maier (Institute of Physics and Physical Society, London, 1982), p. 375.

[12]G. C. Ball, O. Hausser, T. K. Alexander, W. G. Davies, T. S. Forster, I. V. Mitchell, J. R. Beene, D. Horen, and W. McLatchie, Nucl. Phys. A349, 271 (1982).

[13]M. S. Pandey, J. B. Garg, and J. A. Harvey, Phys. Rev. C 15, 600 (1977).

[14]R. L. Macklin, R. W. Ingle, and J. Halperin, Nucl. Sci. Eng. 71, 205 (1979).

[15]R. L. Macklin and J. H. Gibbons, Phys. Rev. 159, 1007 (1967).

[16]N. M. Larson and F. G. Perey, Oak Ridge National Laboratory Report No. ORNL/TM-7485, 1980.

[17]C. H. Johnson and R. R. Winters, Phys. Rev. C 21, 2190 (1980); 27, 416 (1983).

[18]C. H. Johnson, N. M. Larson, C. Mahaux, and R. R. Winters, Phys. Rev. C 27, 1913 (1983).

[19]R. L. Macklin, Nucl. Sci. Eng. 59, 12 (1976).

[20]E. C. Long, M. R. Patterson, and C. H. Johnson, DCON program, Oak Ridge National Laboratory, 1972.

[21]S. F. Mughabghab, M. Divadeenam, and N. E. Holden, Neutron Cross Sections (Academic, New York, 1981), Vol. 1.

[22]H. S. Camarda, Phys. Rev. C 9, 28 (1974).

[23]L. Koester, K. Knopf, and W. Waschkowski, Z. Phys. A 289, 399 (1979).

[24]R. Abegg and S. K. Datta, Nucl. Phys. A287, 94 (1977).

[25]S. Raman, E. T. Jurney, D. A. Outlaw, and I. S. Towner, Phys. Rev. C 27, 1188 (1983).